FAR-INFRARED SOURCE COUNTS AT 70 AND 160 MICRONS IN *SPITZER* DEEP SURVEYS

H. Dole,[1,2] E. Le Floc'h,[1] P. G. Pérez-González,[1] C. Papovich,[1] E. Egami,[1] G. Lagache,[2]
A. Alonso-Herrero,[1] C. W. Engelbracht,[1] K. D. Gordon,[1] D. C. Hines,[1,3] O. Krause,[1] K. A. Misselt,[1]
J. E. Morrison,[1] G. H. Rieke,[1] M. J. Rieke,[1] J. R. Rigby,[1] E. T. Young,[1] L. Bai,[1] M. Blaylock,[1]
G. Neugebauer,[1] C. A. Beichman,[4] D. T. Frayer,[5] J. R. Mould,[6] and P. L. Richards[7]

ABSTRACT

We derive galaxy source counts at 70 and 160 μm using the Multiband Imaging Photometer for *Spitzer* (MIPS) to map the *Chandra* Deep Field–South (CDF-S) and other fields. At 70 μm, our observations extend upward about 2 orders of magnitude in flux density from a threshold of 15 mJy, and at 160 μm they extend about an order of magnitude upward from 50 mJy. The counts are consistent with previous observations on the bright end. Significant evolution is detected at the faint end of the counts in both bands, by factors of 2–3 over no-evolution models. This evolution agrees well with models that indicate that most of the faint galaxies lie at redshifts between 0.7 and 0.9. The new *Spitzer* data already resolve about 23% of the cosmic far-infrared background at 70 μm and about 7% at 160 μm.

Subject headings: galaxies: evolution — galaxies: statistics — infrared: galaxies

1. INTRODUCTION

The cosmic infrared background (CIB), relic emission of the formation and evolution of the galaxies, peaks in the far-infrared (FIR) in the 60–200 μm wavelength range (Puget et al. 1996; Hauser et al. 1998; Lagache et al. 1999; Gispert et al. 2000; Hauser & Dwek 2001). In the local universe only about a third of the extragalactic emission is released in the FIR (Soifer & Neugebauer 1991). However, the CIB FIR peak accounts for more than half of the total optical/infrared background, indicating strong evolution of galaxy properties toward high FIR output in the past. Characterizing the galaxies responsible for most of the CIB is therefore an important goal of cosmological surveys. Galaxy counts (or number counts) provide a powerful tool to investigate the evolution of the galaxies and their contribution to the CIB.

The cryogenic infrared space missions of the *Infrared Astronomical Satellite* (*IRAS*) and *Infrared Space Observatory* (*ISO*) (see Genzel & Cesarsky 2000 and Dole 2003 for reviews) provided important data on source counts at 60 μm (Hacking & Soifer 1991) and at 100 μm (Rowan-Robinson et al. 1986), and more recently at 90 μm (Kawara et al. 1998, 2004; Efstathiou et al. 2000; Juvela et al. 2000; Linden-Vornle et al. 2000; Matsuhara et al. 2000; Rodighiero et al. 2003) and 170 μm (Kawara et al. 1998, 2004; Puget et al. 1999; Matsuhara et al. 2000; Dole et al. 2001). Mid-infrared (MIR) observation with ISOCAM at 15 μm (Elbaz et al. 1999) are also of great interest, since they are believed to resolve a significant fraction of the CIB into sources (Elbaz 2002). The *Spitzer Space Telescope* (Werner et al. 2004) provides the ability for much deeper and wider area surveys from 3.6 to 160 μm. This paper investigates source counts at 70 and 160 μm from *Spitzer*. A companion paper addresses the MIR source counts at 24 μm (Papovich et al. 2004). The three-band source counts are the basis of new phenomenological models by Lagache et al. (2004).

2. OBSERVATIONS AND DATA REDUCTION

Observations were carried out with the Multiband Imaging Photometer for *Spitzer* (Rieke et al. 2004) in the *Chandra* Deep Field–South (CDF-S) and the Boötes field corresponding to the NOAO Deep Wide Field Survey (NDWFS; Jannuzi & Dey 1999); we also used an engineering MIPS observation of the Marano field. The observational mode (scan map) provides multiple sightings of each source, typically 10 and 60 at 70 μm in the Boötes and CDF-S, respectively. However, at 160 μm, the number of sightings is only typically 2 in Boötes and 12 in CDF-S. See Table 1 and Papovich et al. (2004) for details.

The data were reduced with the Data Analysis Tool (Gordon et al. 2004), from the raw data (ramps) to the final coadded mosaics. The illumination corrections were derived from the data themselves. At 70 μm, the data have been median-filtered in the time domain before mosaicking. Note that data from Ge : Ga detectors are always challenging to process; but with MIPS, most of the difficulties are overcome with frequent calibrations (stimulator flashes), which track the responsivity variations. Nevertheless, the noise properties at faint fluxes are still being investigated at both 70 and 160 μm. In this work, we adopt conservative detection limits. A future paper will address extracting the ultimate sensitivity from these data. Sample images in the CDF-S are shown in Figure 1 (Plate 1).

3. PHOTOMETRY AND CATALOGS

To control the sample and the selection function, we accepted source detections only where the redundancy was high (typically 80% or more of the mean weight), avoiding the

[1] Steward Observatory, University of Arizona, 933 North Cherry Avenue, Tucson, AZ 85721.
[2] Institut d'Astrophysique Spatiale, bât 121, Université Paris-Sud, F-91405 Orsay Cedex, France.
[3] Space Science Institute, 4750 Walnut Street, Suite 205, Boulder, CO 80301.
[4] Michelson Science Center, California Institute of Technology, Pasadena, CA 91125.
[5] *Spitzer* Science Center, California Institute of Technology, Pasadena, CA 91125.
[6] NOAO, 950 North Cherry Avenue, Tucson, AZ, 85719.
[7] Department of Physics, 345 Birge Hall, University of California, Berkeley, CA 94720.

TABLE 1
Log of Observations

		70 μm			160 μm		
Field Name [a]	MIPS AOT [b]	Area (deg^2)	t_{int} [c] (s)	S_{cut} [d] (mJy)	Area (deg^2)	t_{int} [c] (s)	S_{cut} [d] (mJy)
Boötes	Med.	8.75	40	80	7.70	8	... [e]
Marano	Slow	0.42	100	25	0.31	20	50
CDF-S	Slow	0.67	600	15	0.54	120	50

[a] See Papovich et al. (2004) for details on fields.
[b] Scan map mode.
[c] Per sky pixel.
[d] Flux density at which catalog was cut.
[e] Field data not used at 160 μm.

edges and the noisiest areas of the images. The resulting positions were fed to DAOPHOT (Stetson 1987) in IRAF[8] for PSF fitting. We checked that the residual maps were indeed free of sources.

At 70 μm the photometric calibration is derived from many observation campaigns, and its uncertainty is conservatively estimated at the order of 20%. We use only detections at 15 mJy and brighter in the CDF-S, 25 mJy and brighter in Marano, and 80 mJy and brighter in the Boötes field. These flux levels are determined using the sharp decrease in the counts due to the incompleteness effect. At 160 μm, the calibration is based on a combination of observations of standard stars, asteroids, and comparisons with measurements with other FIR missions (*ISO*, *COBE*, and modeling including *IRAS* measurements). It is also estimated to be accurate to about 20%. We have included in our counts only objects of 50 mJy and brighter in the CDF-S and Marano (levels determined using incompleteness as at 70 μm). Because of the low redundancy level of the 160 μm data in the Boötes field, we postpone using it for a later paper.

Catalogs were produced separately at each wavelength; surveys at each wavelength are thus *unbiased*. Detected FIR sources in the CDF-S sort as follows. For sources selected at 70 μm, 92% have a 24 μm ID; 54% have a 160 μm ID (same with 24 and 160). For sources selected at 160 μm, 98% have a 24 μm ID; 43% have a 70 μm ID (same with 24 and 70).

4. SOURCE COUNTS

At 70 μm, 131 sources were detected down to 15 mJy in the CDF-S, 55 sources down to 25 mJy in Marano, and 117 down to 80 mJy in the Boötes. At 160 μm, down to 50 mJy, 123 sources were detected in the CDF-S, and 89 sources in Marano. The source density corresponds to about 150 beams per source at 70 μm and 15 at 160 μm, using the definition of Helou & Beichman (1990).

Source counts are given in integral form (Figs. 2a and 3a) and differential form, divided by the Euclidean component (Figs. 2b and 3b) at 70 and 160 μm, respectively.

Note that we did not correct for incompleteness. Error bars on counts are 1 σ Poisson uncertainty. Bins with less than four sources have not been displayed for clarity, since their

significance is low, with uncertainties of 50% or higher. In addition, photometric uncertainty have been displayed at high flux only. In order to visualize the contribution from each field, source counts have not been merged and have been overplotted. One should keep in mind that MIPS source counts will eventually go deeper and will be corrected for incompleteness.

The observed fields nicely complement each other in terms of area and depth. This allows us to probe a flux range of almost 2 orders of magnitude at 70 μm. One order of magnitude is covered at 160 μm. It is possible to check consistency and the cosmic variance in the common flux density range. At 70 μm, in the range 25 to 100 mJy where three fields overlap in flux density, the differential counts are almost consistent within the error bars. At 160 μm, in the range 100 to 300 mJy, the differential counts are consistent within the error bars. At both wavelengths, number counts in CDF-S appear consistently lower than in Marano.

5. DISCUSSION

5.1. 70 μm

The MIPS 70 μm counts show a great consistency with the *IRAS* 60 μm counts of Lonsdale et al. (1990) converted at 70 μm using $\nu_{60}S_{60} = \nu_{70}S_{70}$.

A selection of recent models is shown in Figure 2, including a nonevolution scenario. The most striking result is the strong excess of MIPS 70 μm sources compared to the nonevolution model, a factor of 3 at around 20–30 mJy. Strong evolution had been reported previously at 60 and 90 μm, and these data provide unambiguous confirmation.

Two models lie close to the data: King & Rowan-Robinson (2003) and Lagache et al. (2003, 2004). These models, developed to fit observables mostly from *IRAS*, *ISO*, and SCUBA surveys as well as the CIB spectral energy distribution (SED), are based on a strong evolution of luminous (and ultraluminous) infrared galaxies (LIRGs and ULIRGs, respectively). The latter model predicts a peak in the redshift distributions of resolved sources at 70 μm near $z \sim 0.7$ (Dole et al. 2003). Figure 4a shows the galaxy contribution to the differential counts, as a function of redshift, from the Lagache et al. (2004) model. Between ~ 5 and ~ 100 mJy, sources at $0.7 \leq z \leq 0.9$ contribute the most to the counts. At brighter fluxes (reached by *IRAS* and *ISO*), contributions from local galaxies are more important.

The source counts integrated at 70 μm correspond to a brightness of 0.022 MJy sr^{-1} or 0.95 nW m^{-2} sr^{-1}. The value of the CIB at this wavelength is not known accurately owing to
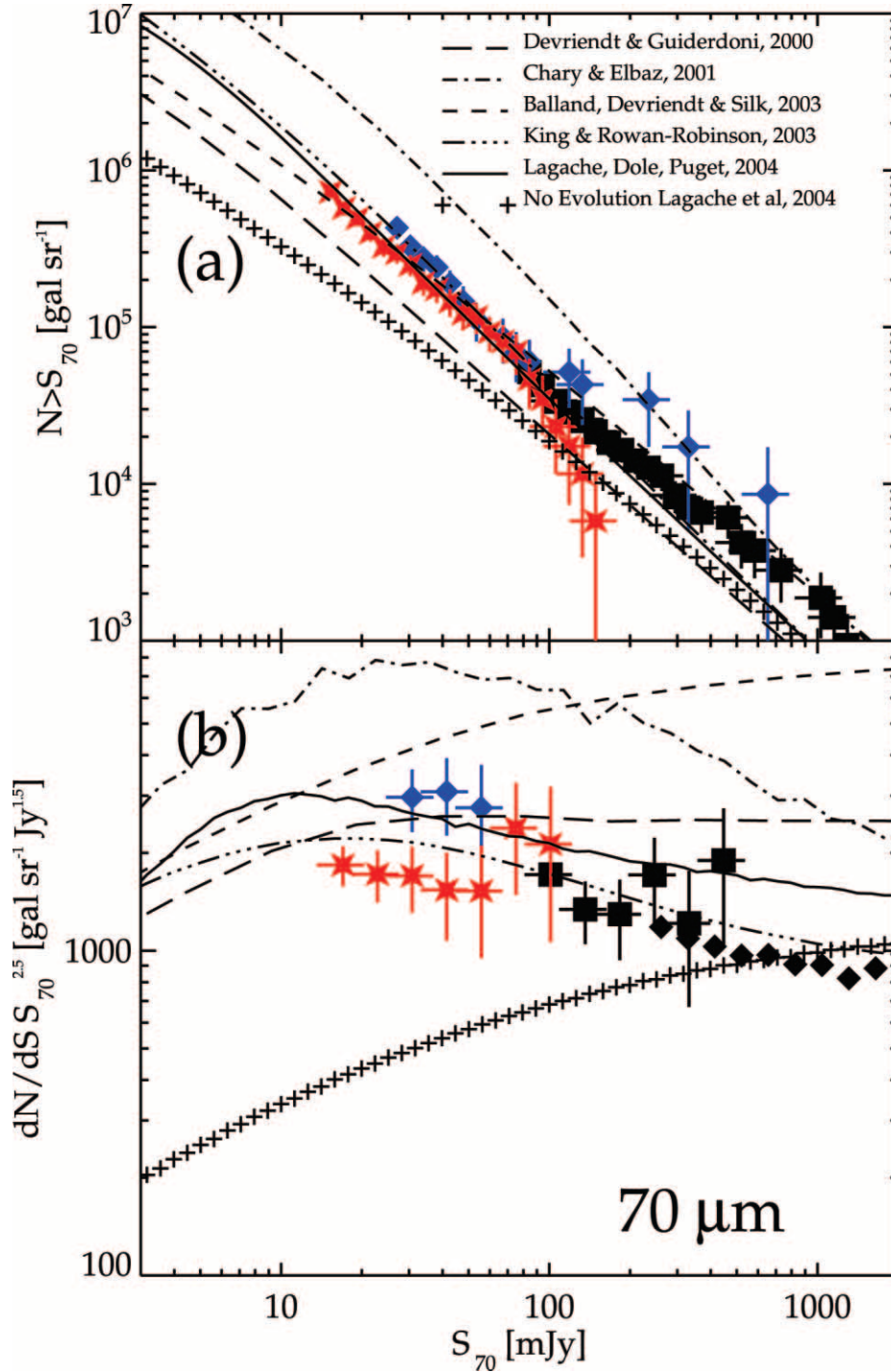
FIG. 2.—Source Counts at 70 μm with no correction for incompleteness. *Red star*, CDF-S; *blue diamond*, Marano; *black square*, Boötes Field; *black diamond*, *IRAS* 60 μm counts from Lonsdale et al. (1990) converted at 70 μm. (*a*) Integral source counts. For clarity, photometric uncertainty is only shown for $S_{70\mu m} >$ 100 mJy. (*b*) Differential source counts. Models are also plotted: *long dashed line*, Devriendt & Guiderdoni (2000); *dash-dotted line*, Chary & Elbaz (2001); *dashed line*, Balland et al. (2003); *dash-dot-dot-dotted line*, King & Rowan-Robinson (2003); *solid line*, Lagache et al. (2004); *plus signs*, no-evolution model.

contamination by zodiacal light. If we use the CIB value from the model of Lagache et al. (2004), the MIPS counts show that at 70 μm about 23% of the 70 μm CIB is already resolved.

5.2. 160 μm

At 160 μm, the comparison with the *ISO* FIRBACK 170 μm survey (Dole et al. 2001) shows that the counts are consistent and within the error bars in the whole common range, 180–

300 mJy. Other *ISO* observations (Matsuhara et al. 2000; Kawara et al. 2004) agree as well.

Figure 3 overplots the same models as at 70 μm. The evolution detected at 170 μm is confirmed at 160 μm, down to fainter levels. At about 100 mJy, an excess of sources by more than a factor of 2 is observed compared to a nonevolution scenario. Interestingly, as for 70 μm, the observed evolution is better fitted by the models of Lagache et al. (2004) and King
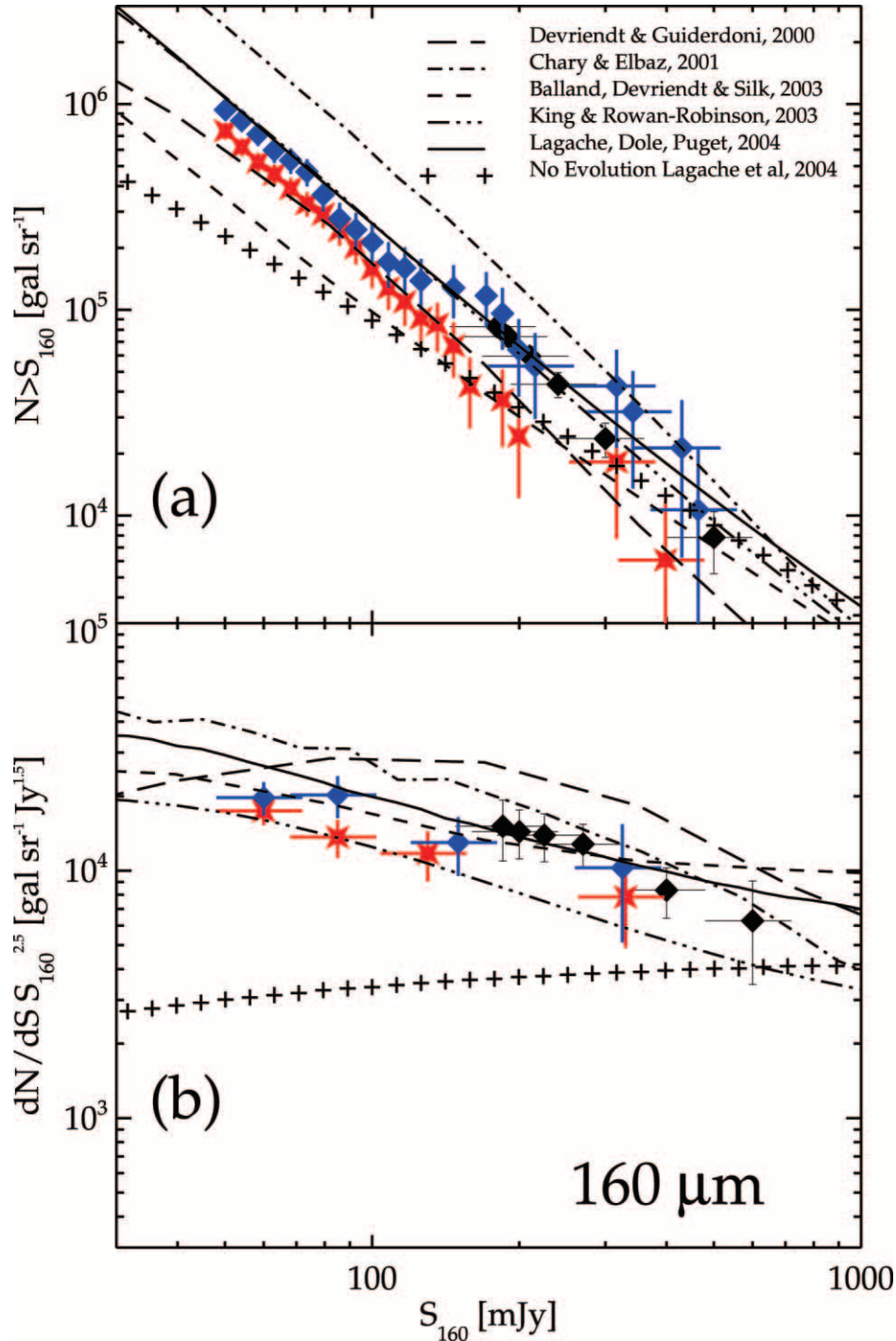
Fig. 3.—Source counts at 160 μm with no correction for incompleteness. *Red star*, CDF-S; *blue diamond*, Marano field; *black diamond*, *ISO* FIRBACK 170 μm counts from Dole et al. (2001). (*a*) Integral source counts. For clarity, photometric uncertainty is only shown for $S_{160\,\mu m} > 200$ mJy. (*b*) Differential source counts. Models are also plotted with the same symbols as Fig. 2.

& Rowan-Robinson (2003). The observed slope also agrees with Mould (2003).

We have constrained the bright end of galaxy number counts at 170 μm by using data from the ISOPHOT Serendipity Survey (ISOSS). ISOSS provides a total sky coverage of 15% and is virtually complete at a flux density level of $S_{170\,\mu m} = 50$ Jy. Based on all optically identified galaxies detected by ISOSS (Krause 2003; Stickel et al. 2004) we have derived an integral number density of $n(S_{170\,\mu m} > 50$ Jy$) =$ 14 $\pm$ 3 gal sr^{-1} galaxies at high Galactic latitudes. This point is perfectly matched by the model of Lagache et al. (2003, 2004).

The most striking result of the models that fit the number counts is the existence of two regimes in flux density. In the *ISO* range (fluxes above 200 mJy) most of the sources contributing to the counts are local; this is confirmed by observation (Patris et al. 2003). At fainter fluxes, between ~10 and 200 mJy, the counts should be dominated by a population located at redshifts between 0.7 and 0.9.

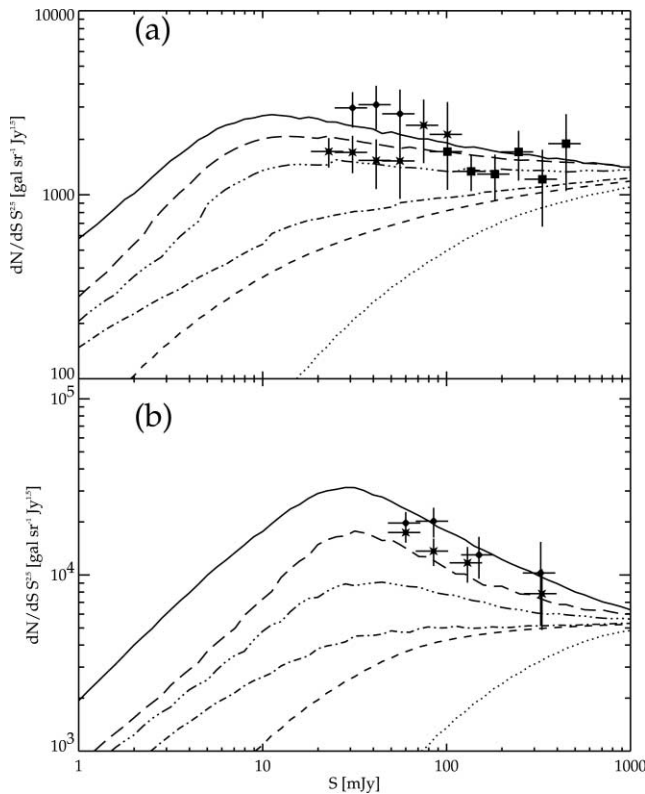FIG. 4.—Cumulative contributions to the differential source counts at 70 and 160 μm of galaxies, as a function of redshift, form the model of Lagache et al. (2004): (*a*) 70 μm; (*b*) 160 μm. Symbols are described in Figs. 2 and 3. Galaxies contributing to the counts at redshifts 0.1 (*dotted line*), 0.3 (*dashed line*), 0.7 (*dot-dashed line*), 0.9 (*triple-dot-dashed line*), and 1.1 (*long-dashed line*). The total contribution is the upper solid line.

The source counts integrated at 160 μm correspond to a brightness of 0.07 MJy sr^{-1} or 1.4 nW m^{-2} sr^{-1}. The CIB value at this wavelength is 1 MJy sr^{-1} (Lagache et al. 2000); the MIPS counts show that at 160 μm about 7% of the CIB is resolved. Since these counts are preliminary, are not corrected for incompleteness, and are subject to cosmic variance, we anticipate that the actual value might be higher.

5.3. *Concluding Remarks*

The first MIPS far-infrared source counts, spanning about 2 orders of magnitude in flux density at 70 μm (and one at 160 μm), are consistent with previous observations on the bright end and show unambiguous evolution on the faint end. Models predict that most of the sources lie at $z \sim 0.7$ with a tail up to $z \sim 2$ (Dole et al. 2003; Lagache et al. 2003, 2004). This work and companion papers on source counts at 24 μm (Papovich et al. 2004), confusion at 24, 70, and 160 μm (Dole et al. 2004), and on the interpretation of these new data from the *Spitzer* cosmological surveys (Lagache et al. 2004) shed new light on the statistical properties of galaxies in an unexplored regime in flux density, and likely in a critical region of redshift space (up to redshifts $z \sim 2$) in the FIR (Egami et al. 2004; Le Floc'h et al. 2004).

REFERENCES

Balland, C., Devriendt, J. E. G., & Silk, J. 2003, MNRAS, 343, 107
Chary, R., & Elbaz, D. 2001, ApJ, 556, 562
Devriendt, J. E. G., & Guiderdoni, B. 2000, A&A, 363, 851
Dole, H. 2003, in Exploiting the *ISO* Data Archive: Infrared Astronomy in the Internet Age, ed. C. Gry, S. Peschke, J. Matagne, P. Garcia-Lario, R. Lorente, & A. Salama (ESA SP-511) (Noordwijk: ESA), 307
Dole, H., Lagache, G., & Puget, J. L. 2003, ApJ, 585, 617
Dole, H., et al. 2001, A&A, 372, 364
———. 2004, ApJS, 154, 93
Efstathiou, A., et al. 2000, MNRAS, 319, 1169
Egami, E., et al. 2004, ApJS, 154, 130
Elbaz, D. 2002, A&A, 384, 848
Elbaz, D., et al. 1999, A&A, 351, L37
Genzel, R., & Cesarsky, C. J. 2000, ARA&A, 38, 761
Gispert, R., Lagache, G., & Puget, J. L. 2000, A&A, 360, 1
Gordon, K. D., et al. 2004, PASP, submitted
Hacking, P. B., & Soifer, B. T. 1991, ApJ, 367, L49
Hauser, M. G., & Dwek, E. 2001, ARA&A, 37, 249
Hauser, M. G., et al. 1998, ApJ, 508, 25
Helou, G., & Beichman, C. A. 1990, in From Ground-Based to Space-Borne Sub-mm Astronomy (ESA SP-314) (Noordwijk: ESA), 117
Jannuzi, B. T., & Dey, A. In Weymann, R. 1999, in ASP Conf. Ser. 191, Photometric Redshifts and High Redshift Galaxies, ed. R. J. Weymann, L. J. Storrie-Lombardi, M. Sawicki, & R. J. Brunner (San Francisco: ASP), 111
Juvela, M., Mattila, K., & Lemke, D. 2000, A&A, 360, 813
Kawara, K., et al. 1998, A&A, 336, L9

Kawara, K., et al. 2004, A&A, 413, 843
King, A. J., & Rowan-Robinson, M. 2003, MNRAS, 339, 260
Krause, O. 2003, Ph.D. thesis, Ruperto-Carola Univ. Heidelberg
Lagache, G., Dole, H., & Puget, J. L. 2003, MNRAS, 338, L555
Lagache, G., Haffner, L. M., Reynolds, R. J., & Tufte, S. L. 2000, A&A, 354, 247
Lagache, G., et al. 1999, A&A, 344, 322
———. 2004, ApJS, 154, 112
Le Floc'h, E., et al. 2004, ApJS, 154, 170
Linden-Vornle, M. J. D., et al. 2000, A&A, 359, L51
Lonsdale, C. J., Hacking, P. B., Conrow, T. P., & Rowan-Robinson, M. 1990, ApJ, 358, L60
Matsuhara, H., et al. 2000, A&A, 361, 407
Mould, J. 2003, ApJ, 587, L93
Papovich, C., et al. 2004, ApJS, 154, 70
Patris, J., Dennefeld, M., Lagache, G., & Dole, H. 2003, A&A, 412, 349
Puget, J. L., et al. 1996, A&A, 308, L5
———. 1999, A&A, 345, 29
Rieke, G. H., et al. 2004, ApJS, 154, 25
Rodighiero, G., et al. 2003, MNRAS, 343, 1155
Rowan-Robinson, M., et al. 1986, MNRAS, 219, 273
Soifer, B. T., & Neugebauer, G. 1991, AJ, 101, 354
Stetson, P. B. 1987, PASP, 99, 191
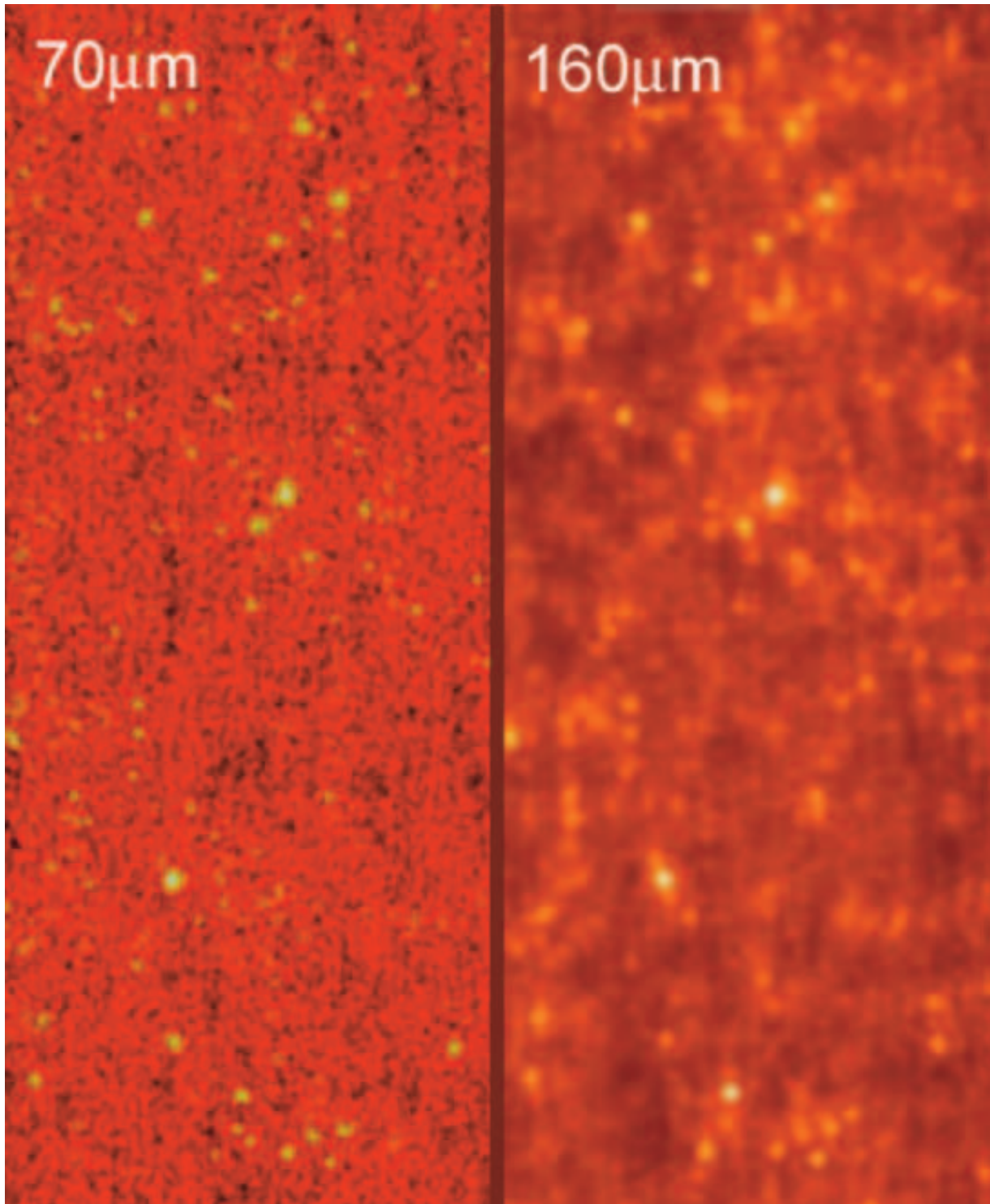Stickel, M., et al. 2004, A&A, in press
Werner, M., et al. 2004, ApJS, 154, 1

FIG. 1.—MIPS observations of the *Chandra* Deep Field–South at 70 and 160 μm. The field covers an area of $25' \times 1°$.

PLATE 1